Modeling elastic waves in the presence of a borehole and free surface

José M. Carcione, *Osservatorio GeoJisico Sperimentale, Trieste, Italy* PP4.3

Summary

We introduce a modeling algorithm to simulate wave propagation through a rotationally symmetric borehole environment in the presence of the earth's surface. The modeling simulates 3-D waves in a multidomain 2-D Chebychev mesh, and requires domain decomposition technique and a special treatment of corner and-joint side points, both based on a characteristic decomposition of the wavefield. The performance of the multidomain mesh is verified in 2-D Cartesian soordinates by solving Lamb's problem. Finally, simulation in an empty borehole for two different frequency ranges shows that the method can handle a model with *a* realistic hole diameter and suitable for reverse VSP configurations.

Introduction

The problem of obtaining a realistic VSP survey by using pseudospectral differential operators was attacked b David Kessler and Dan Kosloff in a series of papers (Kessler an Kosloff, 1990, 1991, 1992). In the first two, they solve for 2-D acoustic and elastic wave propagation in a plane perpendicular to the hole by using Chebychev and Fourier differential o erators in the radial and angular directions, respectively. In the third paper, they add a Fourier expansion in the vertical direction to propagate 3-D wavefields. They simulate a 4 m borehole diameter and propagate a 40 Hz pulse a distance of 300 m from the hole, which is equivalent to a maximum to minimum significant length ratio of 75. On the other hand, Yoon and McMechan (1992) use a staggered finite-difference scheme to simulate full-wavefield sonic logs. They use a realistic hole diameter and propagate a 10 KHz pulse 25 cm from the borehole. However, the challenging problem is to propagate a seismic pulse with a realistic borehole diameter. With resent-day computers, this task seems difficult to accomplish, at least in three dimensions and with realistic computer times.

The present modeling technique solves wave propagation in 3-D rotationally symmetric media. In this context, the azimuthal particle velocity component decouples from the other components. The algorithm is based on a multidomain spectral method which combines 2-D Chebychev meshes. The advantages of this type of mesh is that general boundary conditions can be implemented at the four boundaries of the grid (Carcione 1993a,b), allowing the modeling of the borehole and the Earth's surface. In addition, grid matching handles wave pro agation from one subdomain to the other. Both boundary conditions and domain decomposition are based on characteristics perpendicular to the boundaries. This 2-D approach for modeling 3-D propagation avoids the angular direction grid, which involves very small grid spacings (Kessler and Kosloff, 1992) and therefore very small time steps for the time-integration algorithm.

The wave equation

The wave equation combines the equation of momentum conservation with the constitutive relations for isotropic and elastic media. The velocity-stress formulation below represents either propagation in 2-.D Cartesian coordinates (x,z) or 3-D propagation in cylindrical coordinates (r, ϕ, z), where axially symmetric borehole, formation and source are assumed. In this case, the wavefield does not depend on the azimuthal variable ϕ.

$P-S$ -- propagation

$$\frac{\partial v_r}{\partial t} = \frac{1}{\rho}\left(\frac{\partial \sigma_{rr}}{\partial r} + \frac{\partial \sigma_{rz}}{\partial z}\right) + \frac{\gamma}{\rho}(\sigma_{rr} - \sigma_{\phi\phi}) + f_r, \tag{1a}$$

$$\frac{\partial v_z}{\partial t} = \frac{1}{\rho}\left(\frac{\partial \sigma_{rz}}{\partial r} + \frac{\partial \sigma_{zz}}{\partial z}\right) + \frac{\gamma}{\rho}\sigma_{rz} + f_z, \tag{1b}$$

$$\frac{\partial \sigma_{rr}}{\partial t} = E\frac{\partial v_r}{\partial r} + \lambda\left(\frac{\partial v_z}{\partial z} + \gamma v_r\right), \tag{1c}$$

$$\frac{\partial \sigma_{zz}}{\partial t} = E\frac{\partial v_z}{\partial z} + \lambda\left(\frac{\partial v_r}{\partial r} + \gamma v_r\right), \tag{1d}$$

$$\frac{\partial \sigma_{rz}}{\partial t} = \mu\left(\frac{\partial v_z}{\partial r} + \frac{\partial v_r}{\partial z}\right). \tag{1e}$$

$$\frac{\partial \sigma_{\phi\phi}}{\partial t} = \gamma E v_r + \lambda\left(\frac{\partial v_r}{\partial r} + \frac{\partial v_z}{\partial z}\right). \tag{1f}$$

2-D *Cartesian, (x,z) -- plane: $r = x$, $\gamma = 0$, $\sigma_{\phi\phi} = 0$,*

3-D *Cylindrical:* $\gamma = 1/r$,

SH - propagation (torsional waves)

$$\frac{\partial v_\phi}{\partial t} = \frac{1}{\rho}\left(\frac{\partial \sigma_{r\phi}}{\partial r} + \frac{\partial \sigma_{\phi z}}{\partial z}\right) + 2\frac{\gamma}{\rho}\sigma_{r\phi} + f_\phi, \tag{2a}$$

$$\frac{\partial \sigma_{r\phi}}{\partial t} = \mu\left(\frac{\partial v_\phi}{\partial r} - \gamma v_\phi\right), \tag{2b}$$

$$\frac{\partial \sigma_{\phi z}}{\partial t} = \mu\frac{\partial v_\phi}{\partial z}, \tag{2c}$$

2-D *Castesian, (x,z) - plane: $r = x, \phi = y, \gamma = 0$,*

3 -D Cylindrical: $\gamma = 1/r$.

In the preceding equations, $E = \lambda + 2\mu$, with λ and μ the Lame' constants; v are the particle velocities, σ are the stress components, ρ denotes the density, and f are the body forces per unit volume.

The Numerical Method

Each computational subdomain is a square region where the grid distribution is defined by the Gauss-Lobatto points ζ. The spatial derivatives are compute via a variant of the fast Fourier transform (FFT) for the cosine transform. The distribution of the grid points can be altered conveniently by 1-D) stretching transformations. In the exam les presented here the following stretching function is used (Kosloff et al., 1990):

$$f(\zeta) = -|p|^{-1/2}\sin^{-1}\left(\frac{2p\zeta + 4}{\sqrt{q^2 - 4p}}\right), \tag{3}$$

where $p = 0.5\alpha^{-2}(\beta^{-2} + 1) - 1$ and $q = 0.5\alpha^{-2}(\beta^{-2} - 1)$. It can be seen that the amount of grid stretching at $\zeta = -1$ is $df/d\zeta = \alpha$, and that the stretching at $\zeta = 1$ is $df/d\zeta = \alpha\beta$.

The 2-D Chebychev operator is very sensitive to the boundary conditions. Stabilization of the algorithm is based on a characteristic treatment of the wavefield at the boundaries of each subdomain. The wavefield is decomposed into one-way modes (or characteristics) perpendicular to the boundaries, and the incoming modes are modified according to the particular boundary condition, In this work, the multidomain shown in Figure 1 is used. The directions of the characteristics are also represented. Corners points, like L, for instance, were tested in a previous work Carcione, 1993a,b). Problems may arise from the so-called 'I points, which combine interface and free surface boundary conditions (T 1), or interface and non-reflecting boundary conditions (T2). These points are treated independently (in each subdomain) with rotated characteristics, Unlike the interface points, where the wavefield is unique for both subdomains, T points have dissimilar values.

The stress-free and non-reflecting boundary equations for the upper and lower boundaries of each subdomain, respectively, corresponding to equations (la-f) are now described.

The **stress-free** boundary equations are:

$$v_r^{(new)}(\cdot) = v_r^{(old)}(\cdot) + \frac{1}{Z_S}\sigma_{rz}^{(old)}(\cdot), \tag{4a}$$

$$v_z^{(new)}(\cdot) = v_z^{(old)}(\cdot) + \frac{1}{Z_P}\sigma_{zz}^{(old)}(\cdot), \tag{4b}$$

$$\sigma_{rr}^{(new)}(\cdot) = \sigma_{rr}^{(old)}(\cdot) - \frac{\lambda}{E}\sigma_{zz}^{(old)}(\cdot), \tag{4c}$$

$$\sigma_{zz}^{(new)}(\cdot) = 0, \tag{4d}$$

$$\sigma_{rz}^{(new)}(\cdot) = 0, \tag{4e}$$

$$\sigma_{\phi\phi}^{(new)}(\cdot) = \sigma_{\phi\phi}^{(old)}(\cdot) - \frac{\lambda}{E}\sigma_{zz}^{(old)}(\cdot), \tag{4f}$$

where $(\cdot)$ indicates either subdomain A or subdomain B, and $Z_P = \sqrt{E\rho}$, $Z_S = \sqrt{\mu\rho}$ are the compressional and shear impedances of the medium. The superscripts *(old)* and *(new)* refer to the field variables before and after the modification of the incoming characteristics, respectively. This is done at each time step.

The **non-reflecting** boundary equations are:

$$v_r^{(new)}(\cdot) = \frac{1}{2}\left[v_r^{(old)}(\cdot) - \frac{1}{Z_S}\sigma_{rz}^{(old)}(\cdot) \right], \tag{5a}$$

$$v_z^{(new)}(\cdot) = \frac{1}{2}\left[v_z^{(old)}(\cdot) - \frac{1}{Z_P}\sigma_{zz}^{(old)}(\cdot) \right], \tag{5b}$$

$$\sigma_{rr}^{(new)}(\cdot) = \sigma_{rr}^{(old)}(\cdot) - \frac{\lambda}{2E}\left[\sigma_{zz}^{(old)}(\cdot) + Z_P v_z^{(old)}(\cdot) \right], \tag{5c}$$

$$\sigma_{zz}^{(new)}(\cdot) = \frac{1}{2}\left[\sigma_{zz}^{(old)}(\cdot) - Z_P v_z^{(old)}(\cdot) \right], \tag{5d}$$

$$\sigma_{rz}^{(new)}(\cdot) = \frac{1}{2}\left[\sigma_{rz}^{(old)}(\cdot) - Z_S v_r^{(old)}(\cdot) \right], \tag{5e}$$

$$\sigma_{\phi\phi}^{(new)}(\cdot) = \sigma_{\phi\phi}^{(old)}(\cdot) - \frac{\lambda}{2E}\left[\sigma_{zz}^{(old)}(\cdot) + Z_P v_z^{(old)}(\cdot) \right]. \tag{5f}$$

The stress-free equations for the left boundary of A are obtained from (4a-f) by substituting $r \to z$, $z \to r$. Similarly, the non-reflecting equations for the right boundary of suddomain B are obtained from (4a-l).

The vertical interface separating the subdomains can be a real material interface or just a boundary separating regions of the same medium. As before, the wave equation is decomposed into wave modes describing outgoing and incoming wave modes perpendicular to the boundary. The outgoing waves are determined by the solution inside the subdomain, while the incoming waves are calculated from the conditions at the interface, i.e., continuity of displacements and normal stresses. The **interface** boundary equations (e.g., Carcione, 1991; Tessmer et al,, 1992) are given by

$$v_r^{(new)} = C_P\left[Z_P(B)v_r^{(old)}(B) + Z_P(A)v_r^{(old)}(A) - \sigma_{rr}^{(old)}(A) + \sigma_{rr}^{(old)}(B) \right],$$

$$v_z^{(new)} = C_S\left[Z_S(B)v_z^{(old)}(B) + Z_S(A)v_z^{(old)}(A) - \sigma_{rz}^{(old)}(A) + \sigma_{rz}^{(old)}(B) \right],$$

$$\sigma_{rr}^{(new)} = C_P Z_P(A)Z_P(B)\left[v_r^{(old)}(B) - v_r^{(old)}(A) + \frac{\sigma_{rr}^{(old)}(A)}{Z_P(A)} + \frac{\sigma_{rr}^{(old)}(B)}{Z_P(B)} \right],$$

$$\sigma_{rz}^{(new)} = C_S Z_S(A)Z_S(B)\left[v_z^{(old)}(B) - v_z^{(old)}(A) + \frac{\sigma_{rz}^{(old)}(A)}{Z_S(A)} + \frac{\sigma_{rz}^{(old)}(B)}{Z_S(B)} \right],$$

$$\sigma_{zz}^{(new)}(\cdot) = \sigma_{zz}^{(old)}(\cdot) + \frac{\lambda(\cdot)}{E(\cdot)}\left[\sigma_{rr}^{(new)} - \sigma_{rr}^{(old)}(\cdot) \right],$$

$$\sigma_{\phi\phi}^{(new)}(\cdot) = \sigma_{\phi\phi}^{(old)}(\cdot) + \frac{\lambda(\cdot)}{E(\cdot)}\left[\sigma_{rr}^{(new)} - \sigma_{rr}^{(old)}(\cdot) \right], \tag{6a-f}$$

where $C_P = 1/\left[Z_P(A) + Z_P(B) \right]$ and $C_S = 1/\left[Z_S(A) + Z_S(B) \right]$. For the L and 'T' points we use an ad hoc treatment suggested by Lie (1991), who defines the 'normal to the point' inwards and bisecting the angle between the adjacent boundary lines. This procedure involves rotation of the characteristic by an angle n/4.

The boundary and interface equations for SH propagation are similar but more simple than the equations for $P - S$ propagation. The characteristics for the right and left. boundaries are $v_\phi \pm \sigma_{r\phi}/Z_S$ and $\sigma_{\phi z}$, and for the upper and lower boundaries, $v_\phi \pm \sigma_{\phi z}/Z_S$ and $\sigma_{r\phi}$. The equations are given by

Stress-free (upper boundary):

$$v_\phi^{(new)}(\cdot) = v_\phi^{(old)}(\cdot) + \frac{1}{Z_S(\cdot)}\sigma_{\phi z}(\cdot)^{(old)},$$

$$\sigma_{r\phi}^{(new)} = \sigma_{r\phi}^{(old)}, \qquad \sigma_{\phi z}^{(new)} = 0. \tag{7a-c}$$

Non-reflecting (lower bounda t-y):

$$v_\phi^{(new)}(\cdot) = \frac{1}{2}\left[v_\phi^{(old)}(\cdot) - \frac{1}{Z_S(\cdot)}\sigma_{\phi z}(\cdot)^{(old)} \right], \qquad \sigma_{r\phi}^{(new)} = \sigma_{r\phi}^{(old)},$$

$$\sigma_{\phi z}^{(new)}(\cdot) = \frac{1}{2}\left[\sigma_{\phi z}^{(old)}(\cdot) - Z_S(\cdot)v_\phi(\cdot)^{(old)} \right]. \tag{8a-c}$$

As before, the stress-free and non-reflecting equations for the right and left boundaries, respectively, are obtained from (7) and (8) by substituting $r \to z$, and vice-versa.

Interface:

$$v_\phi^{(new)} = C_S\left[Z_S(B)v_\phi^{(old)}(B) + Z_S(A)v_\phi^{(old)}(A) - \sigma_{r\phi}^{(old)}(A) + \sigma_{r\phi}^{(old)}(B) \right],$$

$$\sigma_{r\phi}^{(new)} = C_S Z_S(A)Z_S(B)\left[v_\phi^{(old)}(B) - v_\phi^{(old)}(A) + \frac{\sigma_{r\phi}^{(old)}(A)}{Z_S(A)} + \frac{\sigma_{r\phi}^{(old)}(B)}{Z_S(B)} \right],$$

$$\sigma_{\phi z}^{(new)}(\cdot) = \sigma_{\phi z}^{(old)}(\cdot). \tag{9a-c}$$

Wave propagation in a 2-D Cartesian grid

The example tests the performance of the boundary treatment on T points, in particular on the intersection of the vertical interface with the free surface (point Tl) (see Figure 1). We consider the medium homogeneous with compressional and shear velocities of $c_P = \sqrt{E/\rho}$ = 2000 m/s and $c_S = \sqrt{\mu/\rho}$ = 1300 m/s, respectively, and a density of ρ = 1 g/cm³. The source is a vertical force having a Ricker wavelet time-history with central frequency f_0 = 16 Hz. The force is in subdomain A at 1.87 m depth, and 372.8 m from the interface. A receiver is located in subdomain B at 12 1 m from the interface, and at 212.8 m depth. The example is basically Lamb's problem, for which a closed analytical solution exists.

The calculations use a numerical mesh with N_x = 8 1 and N_z = 121 for each subdomain. Their dimensions after the stretching are x_{max} = 1460.3 m and z_{max} = 2252.3 m, with maximum grid size of $dx_{max} = dz_{max}$ = 20 m at the centers of the meshes. The stretching parameters are a, = 4.86, a, = 7.2 and β = 2. We found from numerical tests that in order to maintain stability, the aspect ratio of the cells (maximurn to minimum length), close to L and T points, must be less than 5. The solution is propagated to 0.8 s with a time step of 1 *ms*, using a 4th-order Runge-Kutta integration scheme. Figure 2 shows a snapshot of the particle velocity vector, and compares numerical and analytical time histories at the receiver. As can be seen from the pictures, the result is satisfactory.

Wave propagation in a cylindrical grid

In this problem we solve equations (la-f) on a cylindrical grid for an empty borehole of diameter 20 cm. The grid and boundary conditions are shown in Figure 1. The left side of subdomain A sitnulates the boreholc wall, and the upper part of the subdomains the surface of the earth. The medium is homogeneous with wave velocities and density as in the previous example. The problem is solved in two different frequency ranges with source central frequencies of 1.5 Kl lz and 400 Hz, corresponding to the acoustic logging and reservoir seismic prospecting bands, respectively.

Figure 3 shows the mesh for the acoustic logging run. The number of grid points in the vertical direction is 121, and in the radial directions 49 (subdomain A) and 121 (subdomain B). The vertical distance is 15 m, and the radial extensions of A and B are 1.2 m and 6 m, respect ivcly. In order to keep the algorithm stable when applying the characteristic treatment, we choose the ratio between the interior and the exterior radii of both meshes less than 80

(Kessler and Kosloff, 1990). The stretching parameters are 2.88 = 7.2 and . The minimum to maximum significant length ratio (radial extent over the borehole radius) is 73, and the radial distance is 8.4 shear wavelengths. A vertical force is applied at 2.7 mm from the borehole wall (a ring-shaped source) and at 1.6 m from the surface. The time stc used by the Runge-Kutta scheme is 5 1O-^{4} ms. Snapshots of the wavcfield are dis played in Figure 3. The waves traveling through the borehole wall and the Rayleigh surface waves have very high amplitude (actually, they are cli ppcd in the second snapshot).

The second model has a vertical distance of 50 m, and radial extensions of 1.2 m and 50 m, rcspcctivel , for subdomains A and *B* The stretching (3) is only applied to the radial direction of the inner mesh, with $\alpha_r(A) = 2.88$ and $\beta = 2$. In this problem, the minimum to maximum length ratio is 513, and the radial distance is 16 shear wavelengths. As before, a vertical ring-shaped source is applied (clamped) to the borehole wall , at 13 m from the surface. A snapshot of the particle velocity vector is shown in Figure 4, where the different waves can be appreciated: R (Rayleigh), T (borehole wave), P (coniprcssional) an S (shear). Finally, Figure 5 displays the seismogram recorded at the borehole wall and surface. It can be seen that, at the surface, the wave T generates a Rayleigh wave R and a new borehole wave propagating downwards (also labeled T in the Figure).

Conclusions

The present modeling scheme is designed to investigate wave phenomena in borehole environments; in particular, waves propagating through the well system and reverse VSP configurations. Since we solve 3-D propagation with the same effort as 2-D modeling, borehole waves and their interaction with the surface can be simulated with realistic computer times. The examples involve an empty hole in a homogeneous formation, but, the borehole fluid can easily be modeled by adding a third subdomain. The numerical scheme can be improved by considering different time steps for each subdomain, thus resulting in a reduction of computer time. The Performance of the L and T points can be irnproved by applying alternative characteristic a roaches. Moreover, the use of genera ized coordinates (Carcione, 1993 allow the modeling of surface topogra hy and variable hole diameter. Realistic material rheology (ane asticity and anisotropy) can be easily incorporated in the modeling (e.g., Carcionc, 1992, 1993b; Tessmer and Behle, 1992).

Although the model has rotational symmetry, it allows for lateral variations of material properties, truncated casing, vertical variations in hole diameter, washouts, borehole bottom, etc. For instance, knowledge of" the velocity of the longitudinal and torsional modes propagatmg through a drill-string provides useful information for the data-processing (e.g., Poletto et al., 1992). The drill-tool (including the coup lng joints) and the drill rig (which generates surface waves) are, Tactically, a rotationally symmetric system.

Acknowledgments

This work was supported in part by the Commission of the European Communities under the GEOSCIENCE project.

References

Carcione, J. M., 1991, Domain Decomposition for Wave Propagation Problems, .J. Sci. Computing, 6 , 453-472.

Carcione, J. M., 1992, Modeling anelastic singular surfaces waves in the earth, Geophysics, S7 , 781-792.

Carcione, J. M., 1993a, The wave equation in generalized coordinates, 63rd Ann. Internat. Mtg. Soc. Expl. Geophys., Expanded Abstracts, 1226-1229

Carcione, .J.M., 1993b, A two-dimensional Chebchev differential operator for the wave equation, 55th Ann. Internal,. Mtg. Europ. Assoc. Expl. Geophys., Expanded Abstracts, B054.

Kessler, D., and Kosloff', D., 1990, Acoustic wave propagation in 2-D cylindrical coordinates, Gcophys. J. Int, 103 , 577-587.

Kessler, D., and Koslff, D)., 1991 , Ellastic wave propagation using cylindrical coordinates, Geophysics, 56 , 2080-2089.

Kessler, D., and Kosloff, D., 1992, 3-D Numerical Simulation of a VSP Survey, submitted to Geophysics.

lie , I., 1991, Ocean/Bottom Acoustic Interaction with Arbitrary Bottom Profile, FFI/Rapport-9 I /7009. NDRE, 1991. 37 , 70-92.

Poletto, F., Angeleri, G., Persoglia, and Carrion, I'.! 1992, Tomographic inversion in drill-bit experiment, 54th Ann. Internat. Mtg. Europ. Assoc. Expl. Geophys., Expandcd Abstracts, P027.

Tessmer, E, Kessler, D., Kosloff, D., and Behle, A., 1992, Multi-domain Chebychev-Fourier Method for the Solution of the Equatiotls of Motion of Dynamic Elasticty, .J. Comput. Phys., 100, 355-363.

Tessmer, E.., and Behle, A., 1992, 3D seismic modelling of general material anisotropy in the presence of the free surface by a Chebychev spectral method, 4th Ann. Internat. Mtg. Europ. Assoc. Expl. Geophys., Expaded Abstracts, B028.

Yoon, K. H., and McMechan, G. A., 1992, 3-D finite-diffcrcncin modeling of elastic waves in borehole environments, Geophysics, 57, 793-804.

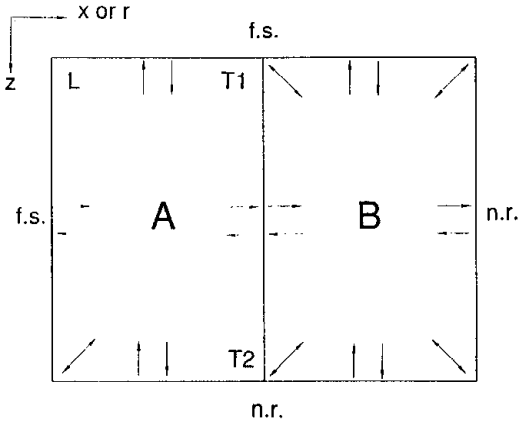

Fig ure 1. Cartesian or cylindrical mesh composed of two Chebychev subgrids (A and B). The directions of the characteristics are indicated The left and upper boundaries satisfy stress-free boundary conditions, and the right and lower boundaries non-reflecting boundary conditions.

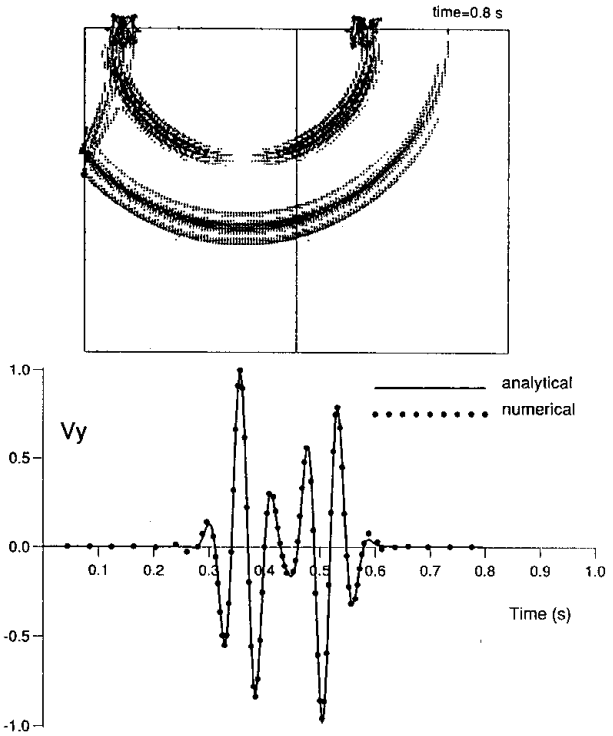

Figure 2. Snapshot of the particle velocity vector for Lamb's problem and comparisen between numerical and analytical solutions. The source is in the left subdomain and the receiver is in the right subdomain.

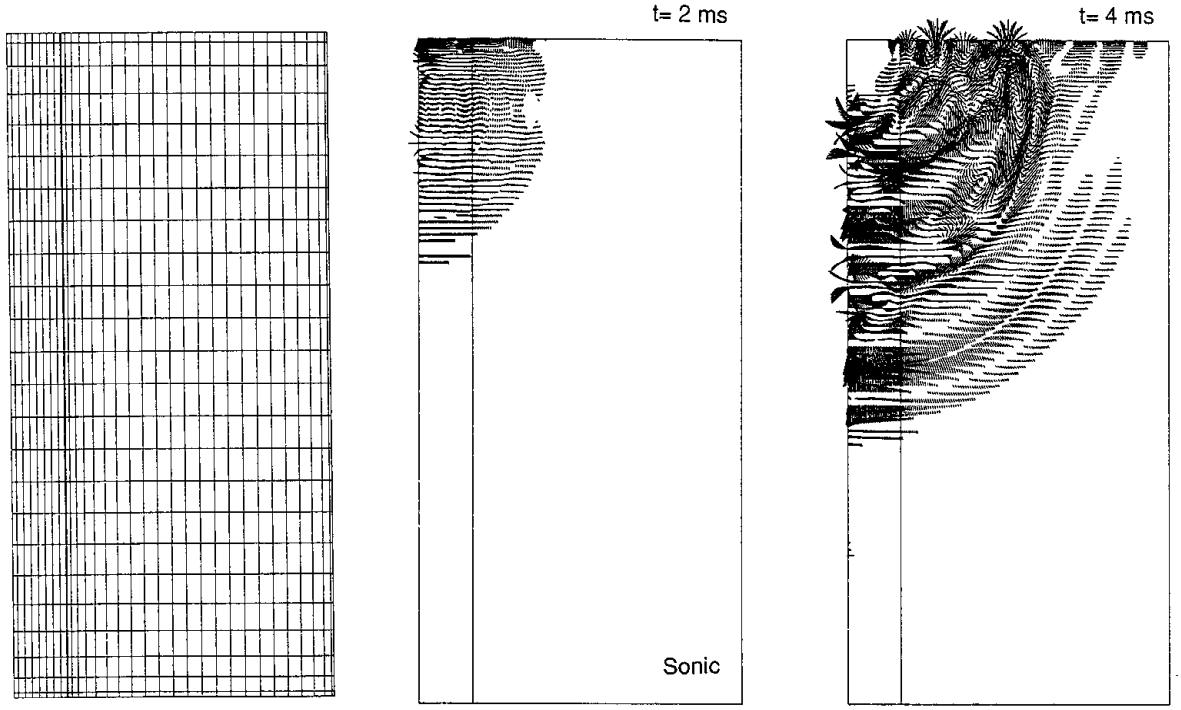

Figure 3. Mesh and snapshots of the particle vctocity vector for the acoustic logging run (3 KHz central frequency source).

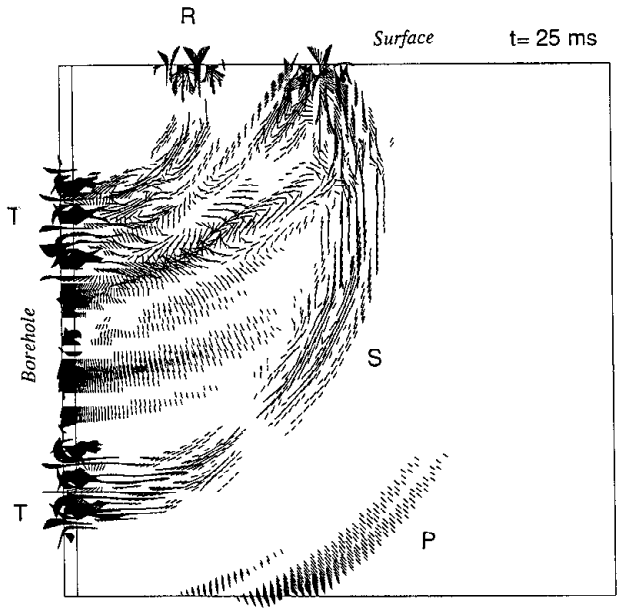

Figure 4. Snapshot of the particle velocity vector for the seismic problem with borehole (800 Hz central frequency source). R denote the Rayleigh wave, 'T' the borchote wave, P the body compressional, and S the shear body wave.

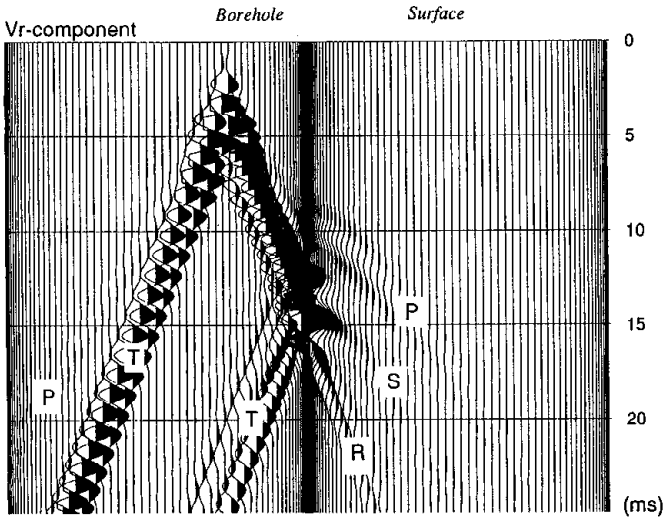

Figure 5. Seismogratn recorded at the borehole wall and earth's surface, corresponding to the seismic problem.